

Quantum versus classical effects at zero and finite temperature in the quantum pyrochlore $\text{Yb}_2\text{Ti}_2\text{O}_7$

Hitesh J. Changlani¹

¹*Department of Physics and Astronomy, Johns Hopkins University, Baltimore, MD 21218 and Institute for Quantum Matter, Johns Hopkins University, Baltimore, MD 21218*
(Dated: May 21, 2018)

We study the finite temperature properties of the candidate quantum spin ice material $\text{Yb}_2\text{Ti}_2\text{O}_7$ within the framework of an anisotropic nearest-neighbor spin 1/2 model on the pyrochlore lattice. Using a combination of finite temperature Lanczos and classical Monte Carlo methods, we highlight the importance of quantum mechanical effects for establishing the existence and location of the low-temperature ordering transition. We perform simulations of the 32 site cluster, which capture the essential features of the specific heat curve seen in the cleanest known samples of this material. Focusing on recent experimental findings [A. Scheie et al., Phys. Rev. Lett. 119, 127201 (2017) and J. D. Thompson et al., Phys. Rev. Lett. 119, 057203 (2017)], we then address the question of how the phase boundary between the ferromagnetic and paramagnetic phases changes when subjected to a magnetic field. We find that the quantum calculations explain discrepancies observed with a completely classical treatment and show that $\text{Yb}_2\text{Ti}_2\text{O}_7$ displays significant renormalization effects, which are at the heart of its reentrant lobed phase diagram. Finally, we develop a qualitative understanding of the existence of a ferromagnet by relating it to its counterpart that exists in the vicinity of the classical ice manifold.

Introduction—Frustrated magnets constitute a fertile hunting ground for discovering unconventional states of matter, including spin liquids with topological properties. The presence of multiple competing energy scales is at the heart of several contentious issues - ranging from the precise knowledge of the low-energy effective Hamiltonian to the reliable determination of the low-energy properties. While spin liquids are desirable, "order-by-disorder" effects [1, 2] typically dominate leading to magnetically ordered or valence bond states. However, combined experimental and theoretical efforts determined Hamiltonian parameters for $\text{Yb}_2\text{Ti}_2\text{O}_7$ (YbTO) [3–5], and suggested a quantum spin ice (spin liquid) ground state [6], possibly circumventing the issues above. This phase is qualitatively described as a quantum superposition of configurations in which the spins are constrained to point into or out of tetrahedra of the pyrochlore lattice, with a two-in-two-out "ice rule" [7–9], a schematic of one such configuration is depicted in Fig. 1. Defects (spin flips) in this rule produce a pair of magnetic "monopoles"; the analogy with electrodynamics led to the theoretical prediction of exotic gapless excitations or "photons" [6]. This fuelled several other studies [10–14] to understand the true nature of YbTO.

Real materials always have some disorder; thus it is important to clarify the nature of the ground state theoretically. Multiple works have addressed the issue at the classical level [13–16], but quantum treatments have been limited to mean field theories [17], small clusters [14, 18], high temperature approaches [12, 14, 19] or sign problem free parameter sets [20, 21]; the latter may not represent YbTO.

Here we show, numerically, that quantum calculations of YbTO favor the picture of a ferromagnet (FM) at low temperature. Using the finite temperature Lanczos method (FTLM) [22, 23], on an effective spin 1/2 anisotropic model on the pyrochlore lattice, we find good agreement with the experimentally observed Schottky anomaly centered at 2.4 K, and the approximate location of the transition at low tem-

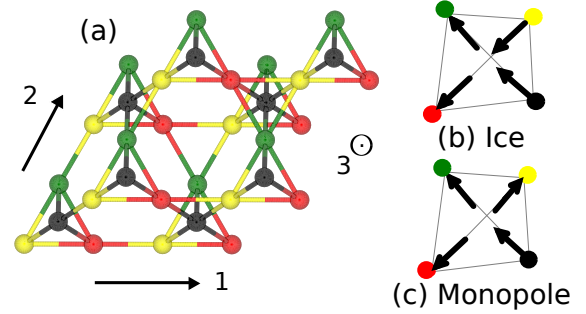


Figure 1. (a) 32 site unit cell of the pyrochlore lattice used for the calculations in the paper, as viewed along the global [111] direction with periodic boundary conditions along the 1,2 and 3 directions. The four colors represent the four FCC sublattices. (b) and (c) show representative configurations of four spins on a single tetrahedron (b) satisfying the two-in two-out ice rule and (c) a monopole associated with a defect in the local ice rule.

perature [16, 24–26]. Our approach complements previous reports [12, 19] on YbTO with the numerical linked cluster (NLC) method. In addition, our calculations in a [111] magnetic field indicate that YbTO has substantial magnetization at small field strengths.

We discuss three main results. First, we demonstrate that quantum effects are crucial for the finite temperature properties of YbTO even for temperatures greater than the ordering temperature T_c ; frustrated interactions and quantum effects renormalize T_c significantly. This complexity is manifest in a magnetic field, and responsible for its unusual reentrant lobed phase diagram [16], thus, an explanation of recent experiments [16, 24, 26] constitute the second purpose of this study. Finally, we present a simple picture in parameter space connecting the ice manifold to the YbTO parameter set, suggesting that the FM obtained within perturbation theory is connected to its counterpart in the non-perturbative regime. For these purposes, we have carried out simulations on 32 sites

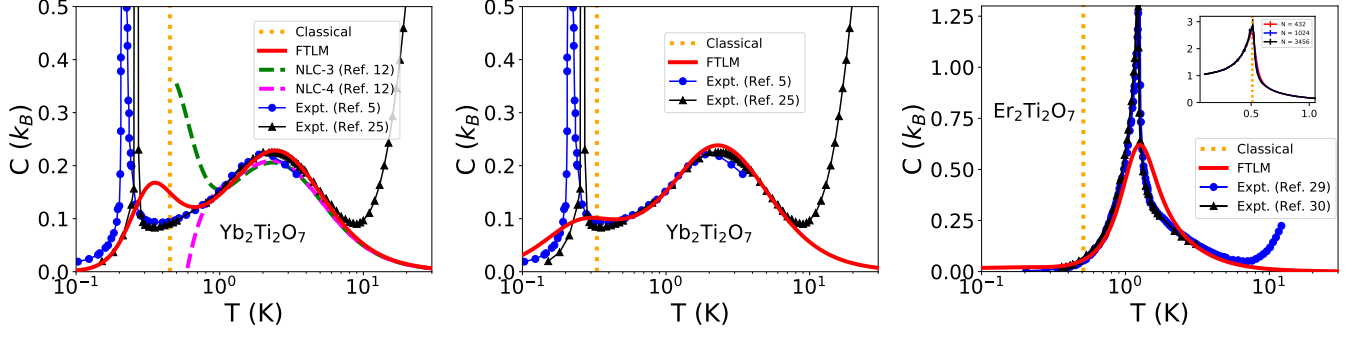


Figure 2. (Color online): Heat capacity (per mole of the magnetic ion) of $\text{Yb}_2\text{Ti}_2\text{O}_7$ and $\text{Er}_2\text{Ti}_2\text{O}_7$ in units of the Boltzmann constant (k_B) as a function of temperature. The theoretical FTLM calculations on the 32 site cluster used model parameters from Ref. [3] and Ref. [24] for $\text{Yb}_2\text{Ti}_2\text{O}_7$ (left and central panels respectively) and Ref. [27] for $\text{Er}_2\text{Ti}_2\text{O}_7$ (right panel). For comparison, results from experimental data sets [5, 25, 28, 29] and previous NLC calculations [12] are shown. The classical estimates of T_c are obtained with classical Monte Carlo, and the results of the profile for $\text{Er}_2\text{Ti}_2\text{O}_7$ are shown in the inset.

as in Fig. 1(a), with a Hilbert space per momentum sector of approximately 536 million, significantly larger than previous quantum treatments [14, 18] on the same model.

The relevant effective spin Hamiltonian including the nearest neighbor interactions and onsite Zeeman coupling to an external magnetic field ($h = (h_x, h_y, h_z)$) is [3, 30, 31],

$$H = \frac{1}{2} \sum_{ij} J_{ij}^{\mu\nu} S_i^\mu S_j^\nu - \mu_B h^\mu \sum_i g_i^{\mu\nu} S_i^\nu \quad (1)$$

where i, j are nearest neighbors and μ, ν refer to x, y, z , S_i^μ refer to the spin 1/2 components at site i , and J_{ij} and g_i are bond and site dependent interaction and coupling matrices respectively, the former characterized completely by four and the latter by two independent parameters. The interaction part is most illuminating when written in terms of spin directions along the local [111] axes (denoted by S),

$$\begin{aligned} H_{int} = & \sum_{\langle i,j \rangle} (2 - \lambda) J_{zz} S_i^z S_j^z - \lambda J_{\pm} (S_i^+ S_j^- + S_i^- S_j^+) \\ & + \lambda J_{\pm\pm} (\gamma_{ij} S_i^+ S_j^+ + \gamma_{ij}^* S_i^- S_j^-) \\ & + \lambda J_{z,\pm} [S_i^z (S_j^+ \zeta_{ij} + S_j^- \zeta_{ij}^*) + i \leftrightarrow j] \end{aligned} \quad (2)$$

where $J_{zz}, J_{\pm}, J_{\pm\pm}, J_{z,\pm}$ are couplings and the parameter λ has been introduced to tune from the classical ice manifold ($\lambda = 0$) to material-relevant parameters ($\lambda = 1$). γ_{ij} and ζ_{ij} are bond dependent phases, the corresponding 4×4 matrices have been written out in the supplementary information. We work with $\lambda = 1$, unless otherwise noted.

Classical versus quantum effects on the specific heat capacity in zero field— We now discuss the results of the temperature dependence of the specific heat of YbTO in zero field using FTLM. This Krylov space method constructs an effective Hamiltonian in the space of suitably chosen vectors (powers of H on a random vector) and calculates observables (that commute with H) from it. The efficiency of FTLM crucially depends on the adequacy of a small number of powers of the

Hamiltonian (M) and a small number of starting random vectors (R) [22, 23, 32]. Some details of the method and its convergence properties are discussed in the supplement.

The leftmost panel of Fig. 2 shows the converged specific heat profile (for the parameters of Ref. [3]) across a wide range of temperatures for $M = 100$ and $R = 160$, along with two experimental data sets [5, 25]. The agreement with the NLC approach at high temperatures is excellent, which serves as a check of our calculations. Importantly, the quantum treatment yields a small "peak" ($T_c \approx 0.34$ K), which appears as a crossover, but is not accessible in the NLC approach [12]. When compared to classical Monte Carlo (MC) simulations, which yield $T_c \approx 0.45$ K, we conclude that T_c is renormalized due to quantum effects (0.11 K is not a small scale for the phenomenon relevant to experiments, as will become clear shortly). Based on finite size analyses (of the MC calculations), the extent of the change in T_c on approaching the thermodynamic limit (TDL) is insufficient to reconcile the classical and quantum estimates.

Prominently, the Schottky anomaly at 2.4 K highlights the importance of quantum effects, since it is *completely* absent from classical simulations in zero field. The agreement of this feature with experiments is remarkable; the deviations are small and not visualized on the scale of the plot. Even below T_c , the numerically computed values essentially lie on top of the experimental data. Above 10 K the experimental data includes contributions from non-magnetic degrees of freedom, not part of the model Hamiltonian.

Recently, different parameters (with reduced J_{zz}) have been reported by Ref. [24]; the central panel of Fig. 2 shows our results for this set. The Schottky anomaly is explained well here too, but importantly a lower T_c is observed, both classically and quantum mechanically; the latter appears as a broad hump at $T_c \approx 0.27$ K. This suggests longer correlation lengths leading to more pronounced finite size effects and YbTO's possible closeness to a phase boundary [13, 14]. However, several aspects of experiments can be understood from the set of Ref. [3] (with smaller finite size effects); we

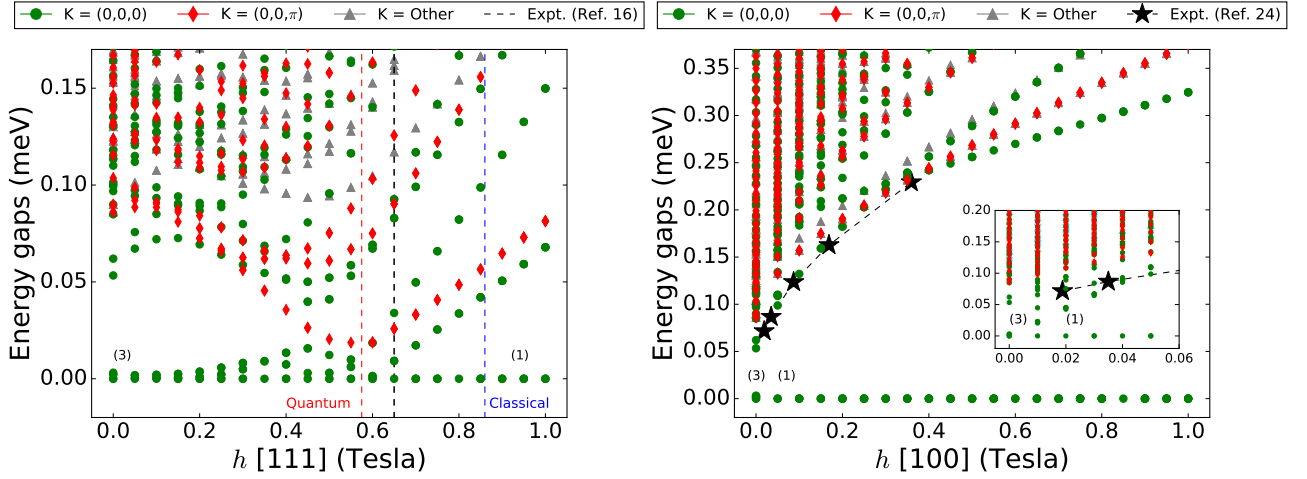


Figure 3. (Color online): Energy (relative to the ground state) versus magnetic field (h) in [111] (left) and [100] (right) directions plotted by momentum sector (k_1, k_2, k_3). $M = 400$ iterations were used for $\mathbf{k} = (0, 0, 0)$ and $\mathbf{k} = (0, 0, \pi)$ and $M = 200$ for the other sectors (denoted by $\mathbf{k} = \text{other}$). k_1 and k_2 directions correspond to translations perpendicular to [111] and the k_3 direction corresponds to translations along [111]. The dashed lines indicate the classical, quantum and experimental estimates of the critical field at zero temperature. There is no phase transition for the [100] direction, although there is reorganization of the energy levels at small fields (inset). The experimental field dependent gap is also shown for the [100] case. For both cases, the quasidegeneracies of the ground state are shown in parentheses.

use those for the remainder of the paper.

While YbTO is the main focus of this work, we demonstrate the effectiveness of the approach for another pyrochlore, $\text{Er}_2\text{Ti}_2\text{O}_7$ (ErTO). ErTO is a candidate for the "order by disorder effect" [1, 2] and has been extensively studied [27, 33–35]. We use the Hamiltonian parameters from Ref. [27], and compare to two experimental data sets [28, 29], our results are in the rightmost panel of Fig. 2. Unlike YbTO, ErTO displays no prominent Schottky anomaly [35], but instead a single phase transition at $T_c = 1.23 \pm 0.01$ K. The quantum calculations capture this effect, and we find $T_c \approx 1.26$ K. In contrast, the MC calculations (see inset for profiles for of systems ranging from 432 to 3456 sites) show a much lower $T_c \approx 0.51(1)$ K.

Low energy spectra and quantum phase transitions in a [111] and [100] magnetic field— The difference between classical and quantum treatments of YbTO is particularly striking at zero temperature, in a [111] magnetic field. Since the Hamiltonian has translational symmetry, all eigenstates have definite momenta $\mathbf{k} = (k_1, k_2, k_3)$; for the 32 site cluster each $k_i = 0$ or $k_i = \pi$. The lowest lying energies are mapped out in all 8 momentum sectors in Fig. 3. Since only momenta $\mathbf{k} = (0, 0, 0)$ and $\mathbf{k} = (0, 0, \pi)$ are involved in the zero temperature phase transition, their corresponding labels have been highlighted, the rest are denoted as " $\mathbf{k} = \text{other}$ ".

In zero field there are three quasidegenerate states, all in $\mathbf{k} = (0, 0, 0)$ followed by two more states separated by approximately 0.05 meV. This is at odds with six quasidegenerate states expected of a cubic FM; this can be attributed to the *lack* of cubic symmetry of the 32 site cluster and the large splittings between states. An analogous effect involving large tunneling between time reversal symmetric odd and even states is also seen on the kagome [36]. For finite fields, only three quasidegenerate states in $\mathbf{k} = (0, 0, 0)$ remain part of the low energy manifold while the other states separate out

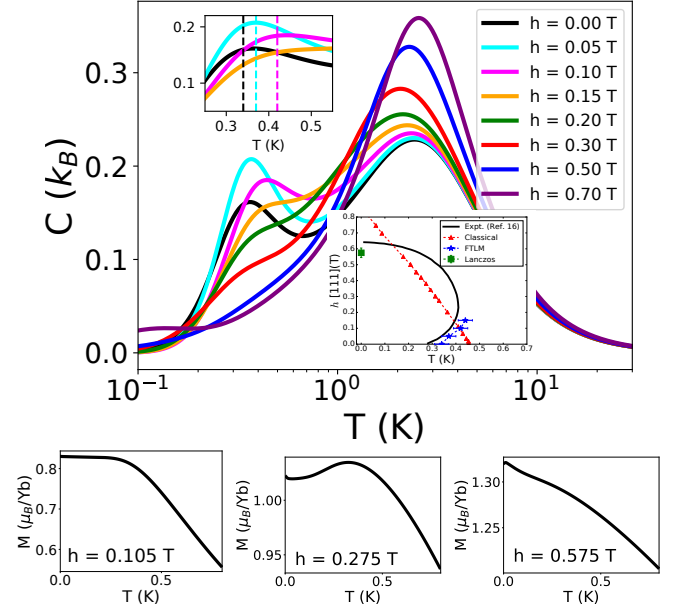


Figure 4. (Color online): The top panel shows the heat capacity (per mole of Yb) in units of the Boltzmann constant (k_B) as a function of temperature for different [111] magnetic field strengths (h). The upper inset zooms in on the low temperature peak; the dashed lines indicate the location of T_c . (For $h \gtrsim 0.15$ T, the peaks are not visible). The lower inset shows the experimental lobed phase diagram and the quantum and classical phase boundaries. The lower panels show the magnetization (M) measured along the [111] direction as a function of temperature for various representative h .

from these. (In the TDL, an infinitesimally small [111] field would gap out three of the six states for a cubic FM). Simultaneously, the lowest $\mathbf{k} = (0, 0, \pi)$ state is lowered in energy. Then between 0.55 to 0.60 T, the lowest $\mathbf{k} = (0, 0, \pi)$ state makes its closest approach to the quasidegenerate manifold;

at this critical field (h_c), the $\mathbf{k} = (0, 0, 0)$ states also split into three branches. The observed h_c agrees well with the experimental value (0.65 T) [16], and is significantly lower than the classical estimate of 0.86(1) T.

In contrast, in a [100] field (right panel of Fig. 3), there is no sign of a phase transition, consistent with the findings of Ref. [24]. At small fields (< 0.03 T), the three quasidegenerate states split (see inset) yielding a single non-degenerate ground state which is qualitatively the same as the high field limit. The trends in the excited eigenenergies also explain the field dependent gap of Ref. [24]. These observations collectively suggest YbTO is a FM.

Specific heat and magnetization in a [111] magnetic field— It is now natural to ask how quantum fluctuations manifest themselves at finite field and temperature. Recently, Ref. [16] found that on increasing the [111] field from 0 to 0.2 T, T_c increased significantly from 0.27 K to 0.42 K, before it gradually decreased towards zero for higher fields, yielding a reentrant lobed phase diagram. While this initial increase is expected of a first order phase transition, the *magnitude* of this effect *could not* be captured classically.

To address this issue, we performed FTLM calculations in a [111] field h ; our results are shown in Fig. 4. (As a compromise between accuracy and computer time, we chose $R = 40$ and $M = 50$). On increasing h , the Schottky anomaly increases in height and the associated entropy increases. Quantum mechanically, the combined entropy of the peak (S_{peak}) and anomaly must be constant ($\ln(2)$ in units of k_B , ignoring non-magnetic contributions), implying S_{peak} decreases with increasing h . Next, the upper inset of Fig. 4 shows the low temperature peaks, marked by dashed lines, the broad features they are associated with move right by ≈ 0.1 K. Both observations agree with experimental findings [16]; the lower inset compares their phase diagram and our simulations.

These inferences are confirmed by the magnetization along the [111] direction (M)

$$M(T, h) = k_B T \frac{\partial \ln Z(T, h)}{\partial h} \quad (3)$$

where $Z(T, h)$ is the partition function directly calculated in FTLM. $M(T, h)$ was evaluated using finite differences; δh was chosen to be 0.01 T for small fields, and 0.05 T for larger fields. Representative results are shown in Fig. 4.

$M(T \rightarrow 0, h)$ is non zero for small h and increases with h suggesting that YbTO is a FM at low temperatures; noting that the distinction between a FM and very good paramagnet (PM) is difficult for a 32 site system (also see supplement) In addition, the quantum simulations show signs of a phase transition from FM to PM, for example a (smooth) kink is seen in $M(T, h)$ up to ≈ 0.15 T. Then for intermediate h ($h \approx 0.15$ T to $h \approx 0.5$ T), M in the putative FM phase is lower than that in the PM, which is consistent with T_c decreasing with increasing h . By 0.55 T, there is no phase transition, consistent with the zero temperature findings.

Relation of YbTO to the ice manifold— We now provide a qualitative interpretation of the existence of an FM by varying

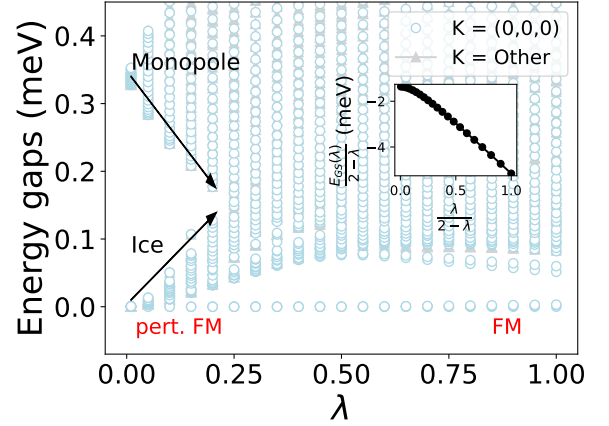


Figure 5. (Color online): Energy (relative to the ground state) versus λ , the parameter defined in the text, that allows us to tune from the classical ice manifold ($\lambda = 0$) to the experimentally relevant parameters ($\lambda = 1$). The inset shows the total ground state energy which smoothly evolves from the perturbative to non-perturbative regime.

λ (in Eq. (2)) from 0 (classical ice) to 1 (YbTO-relevant parameters) and monitoring the spectrum, our results are shown in Fig. 5. When λ is small, perturbative arguments apply due to presence of the gap of order $(2 - \lambda)J_{zz}$. The leading order contribution is to second order; the $J_{z\pm}$ term selects the six FM states [3, 4]. When λ is increased, the energy of the monopole (defect) manifold decreases relative to the highest energy of the ice-like manifold, which itself has split, and around $\lambda \approx 0.25$ the two features meet. However, the ground state is qualitatively unaffected by this high energy feature as the state selection from the ice manifold has already occurred at a much lower energy scale (the inset shows the ground state energy evolving from the perturbative regime to the non-perturbative one). Thus, we suggest that the FM seen in perturbation theory is connected to the FM established earlier in the paper, for the parameters of Ref. [3]. This adiabatic connection suggests YbTO is a near-collinear FM [17, 37].

Conclusion— In summary, quantum mechanical effects are crucial to understanding the zero and finite temperature properties of YbTO. Despite the limitations of finite size (32 sites), we observed good agreement between available experimental data and simulations for a wide range of temperatures. In finite [111] fields, we saw a significant *increase* in T_c of ≈ 0.1 K till ≈ 0.15 T. The presence of substantial magnetization at small fields suggests YbTO is a FM. This picture is strengthened by connecting our results to those known within second order perturbation theory of the ice manifold.

Finally, we showed the utility of FTLM for large Hilbert spaces, for meaningfully studying certain properties of other pyrochlores at finite temperature, as long as the correlation lengths are sufficiently short. One hopes that recent numerical advances at zero and finite temperature [38–45] will push the limits of interesting sizes (of high-dimensional systems) one can go to with some degree of confidence.

Acknowledgements— I thank O. Tchernyshyov and S.

Zhang for teaching me the basics of this field of research and for extensive discussions. I gratefully acknowledge C. Broholm, A. Scheie, J. Kindervater, R.R.P. Singh, R. Coldea, M. Gingras, J. Rau, Y. Wan, K. Plumb, S. Säubert, A. Eyal, S. Koohpayeh, L. Jaubert and B. Clark for useful discussions and D. Kochkov for sharing large-scale exact diagonalization tricks. I thank R.R.P. Singh for sharing his NLC data and for critically reading the first draft of this manuscript, B. Gaulin, A. Hallas and J. Gaudet for providing experimental specific heat data sets from their review article, and A. Scheie and K. Arpino for providing data from their published work. This work was supported through the Institute for Quantum Matter at Johns Hopkins University, by the U.S. Department of Energy, Division of Basic Energy Sciences, Grant DE-FG02-08ER46544. I gratefully acknowledge the Johns Hopkins Homewood High Performance Cluster (HHPC) and the Maryland Advanced Research Computing Center (MARCC), funded by the State of Maryland, for computing resources and Yi Li for sharing part of her computer allocation time.

-
- [1] C. L. Henley, *Phys. Rev. Lett.* **62**, 2056 (1989).
 - [2] J. Villain, R. Bidaux, J.-P. Carton, and R. Conte, *J. Phys. France* **41**, 1263 (1980).
 - [3] K. A. Ross, L. Savary, B. D. Gaulin, and L. Balents, *Phys. Rev. X* **1**, 021002 (2011).
 - [4] L. Savary and L. Balents, *Phys. Rev. Lett.* **108**, 037202 (2012).
 - [5] H. Bloete, R. Wieringa, and W. Huiskamp, *Physica* **43**, 549 (1969).
 - [6] M. Hermele, M. P. A. Fisher, and L. Balents, *Phys. Rev. B* **69**, 064404 (2004).
 - [7] J. D. Bernal and R. H. Fowler, *The Journal of Chemical Physics* **1**, 515 (1933).
 - [8] A. P. Ramirez, A. Hayashi, R. J. Cava, R. Siddharthan, and B. S. Shastry, *Nature* **399**, 333 (1999).
 - [9] S. T. Bramwell and M. J. P. Gingras, *Science* **294**, 1495 (2001).
 - [10] L. Pan, S. K. Kim, A. Ghosh, C. M. Morris, K. A. Ross, E. Kermarrec, B. D. Gaulin, S. M. Koohpayeh, O. Tchernyshyov, and N. P. Armitage, *Nat. Comm.* **5**, 4970 (2014).
 - [11] Y. Wan and O. Tchernyshyov, *Phys. Rev. Lett.* **108**, 247210 (2012).
 - [12] R. Applegate, N. R. Hayre, R. R. P. Singh, T. Lin, A. G. R. Day, and M. J. P. Gingras, *Phys. Rev. Lett.* **109**, 097205 (2012).
 - [13] J. Robert, E. Lhotel, G. Remenyi, S. Sahling, I. Mirebeau, C. Decorse, B. Canals, and S. Petit, *Phys. Rev. B* **92**, 064425 (2015).
 - [14] L. D. C. Jaubert, O. Benton, J. G. Rau, J. Oitmaa, R. R. P. Singh, N. Shannon, and M. J. P. Gingras, *Phys. Rev. Lett.* **115**, 267208 (2015).
 - [15] H. Yan, O. Benton, L. Jaubert, and N. Shannon, *Phys. Rev. B* **95**, 094422 (2017).
 - [16] A. Scheie, J. Kindervater, S. Säubert, C. Duvinage, C. Pfeleiderer, H. J. Changlani, S. Zhang, L. Harriger, K. Arpino, S. M. Koohpayeh, O. Tchernyshyov, and C. Broholm, *Phys. Rev. Lett.* **119**, 127201 (2017).
 - [17] L.-J. Chang, S. Onoda, Y. Su, Y.-J. Kao, K.-D. Tsuei, Y. Yasui, K. Kakurai, and M. R. Lees, *Nat. Comm.* **3**, 992 (2012), article.
 - [18] S. Onoda and Y. Tanaka, *Phys. Rev. B* **83**, 094411 (2011).
 - [19] N. R. Hayre, K. A. Ross, R. Applegate, T. Lin, R. R. P. Singh, B. D. Gaulin, and M. J. P. Gingras, *Phys. Rev. B* **87**, 184423 (2013).
 - [20] N. Shannon, O. Sikora, F. Pollmann, K. Penc, and P. Fulde, *Phys. Rev. Lett.* **108**, 067204 (2012).
 - [21] Y. Kato and S. Onoda, *Phys. Rev. Lett.* **115**, 077202 (2015).
 - [22] J. Jaklic and P. Prelovsek, *Phys. Rev. B* **49**, 5065 (1994).
 - [23] P. Prelovsek and J. Bonca, “Ground state and finite temperature lanczos methods,” in *Strongly Correlated Systems: Numerical Methods*, edited by A. Avella and F. Mancini (Springer Berlin Heidelberg, Berlin, Heidelberg, 2013) pp. 1–30.
 - [24] J. D. Thompson, P. A. McClarty, D. Prabhakaran, I. Cabrera, T. Guidi, and R. Coldea, *Phys. Rev. Lett.* **119**, 057203 (2017).
 - [25] K. E. Arpino, B. A. Trump, A. O. Scheie, T. M. McQueen, and S. M. Koohpayeh, *Phys. Rev. B* **95**, 094407 (2017).
 - [26] V. Peçanha Antonio, E. Feng, Y. Su, V. Pomjakushin, F. Demmel, L.-J. Chang, R. J. Aldus, Y. Xiao, M. R. Lees, and T. Brückel, *Phys. Rev. B* **96**, 214415 (2017).
 - [27] L. Savary, K. A. Ross, B. D. Gaulin, J. P. C. Ruff, and L. Balents, *Phys. Rev. Lett.* **109**, 167201 (2012).
 - [28] P. Dalmas de Réotier, A. Yaouanc, Y. Chapuis, S. H. Curnoe, B. Grenier, E. Ressouche, C. Marin, J. Lago, C. Baines, and S. R. Giblin, *Phys. Rev. B* **86**, 104424 (2012).
 - [29] J. F. Niven, M. B. Johnson, A. Bourque, P. J. Murray, D. D. James, H. A. Dabkowska, B. D. Gaulin, and M. A. White, *Proceedings of the Royal Society of London A: Mathematical, Physical and Engineering Sciences* **470** (2014), 10.1098/rspa.2014.0387.
 - [30] S. H. Curnoe, *Phys. Rev. B* **75**, 212404 (2007).
 - [31] S. Onoda, *Journal of Physics: Conference Series* **320**, 012065 (2011).
 - [32] O. Hanebaum and J. Schnack, *The European Physical Journal B* **87**, 194 (2014).
 - [33] J. Oitmaa, R. R. P. Singh, B. Javanparast, A. G. R. Day, B. V. Bagheri, and M. J. P. Gingras, *Phys. Rev. B* **88**, 220404 (2013).
 - [34] M. E. Zhitomirsky, M. V. Gvozdkova, P. C. W. Holdsworth, and R. Moessner, *Phys. Rev. Lett.* **109**, 077204 (2012).
 - [35] A. M. Hallas, J. Gaudet, and B. D. Gaulin, ArXiv e-prints (2017), arXiv:1708.01312 [cond-mat.str-el].
 - [36] K. Kumar, H. J. Changlani, B. K. Clark, and E. Fradkin, *Phys. Rev. B* **94**, 134410 (2016).
 - [37] Y. Yasui, M. Soda, S. Iikubo, M. Ito, M. Sato, N. Hamaguchi, T. Matsushita, N. Wada, T. Takeuchi, N. Aso, and K. Kakurai, *Journal of the Physical Society of Japan* **72**, 3014 (2003).
 - [38] B. Bruognolo, Z. Zhu, S. R. White, and E. Miles Stoudenmire, ArXiv e-prints (2017), arXiv:1705.05578 [cond-mat.str-el].
 - [39] J. Claes and B. K. Clark, *Phys. Rev. B* **95**, 205109 (2017).
 - [40] H. J. Changlani, J. M. Kinder, C. J. Umrigar, and G. K.-L. Chan, *Phys. Rev. B* **80**, 245116 (2009).
 - [41] A. A. Holmes, H. J. Changlani, and C. J. Umrigar, *Journal of Chemical Theory and Computation* **12**, 1561 (2016).
 - [42] F. R. Petruziello, A. A. Holmes, H. J. Changlani, M. P. Nightingale, and C. J. Umrigar, *Phys. Rev. Lett.* **109**, 230201 (2012).
 - [43] A. A. Holmes, N. M. Tubman, and C. J. Umrigar, *Journal of Chemical Theory and Computation* **12**, 3674 (2016).
 - [44] N. M. Tubman, J. Lee, T. Y. Takeshita, M. Head-Gordon, and K. B. Whaley, *The Journal of Chemical Physics* **145**, 044112 (2016).
 - [45] N. S. Blunt, A. Alavi, and G. H. Booth, *Phys. Rev. Lett.* **115**, 050603 (2015).

Supplemental Material for "Quantum versus classical effects at zero and finite temperature in the quantum pyrochlore $\text{Yb}_2\text{Ti}_2\text{O}_7$ "

I. LOW ENERGY EFFECTIVE HAMILTONIAN

In this section, we discuss details of the relevant spin 1/2 low-energy effective Hamiltonian on the pyrochlore lattice, with nearest neighbor interactions and Zeeman coupling to an external field ($h = (h_x, h_y, h_z)$) [3, 30, 31],

$$H = \frac{1}{2} \sum_{ij} J_{ij}^{\mu\nu} S_i^\mu S_j^\nu - \mu_B h^\mu \sum_i g_i^{\mu\nu} S_i^\nu \quad (\text{S1})$$

where i, j are nearest neighbors and μ, ν refer to x, y, z , S_i^μ refer to the spin components at site i , and \mathbf{J}_{ij} and \mathbf{g}_i are bond and site dependent interactions and coupling matrices respectively (whose components have been written out in Eq. S1). The pyrochlore lattice has four sublattices which we label as 0, 1, 2, 3 and we take the relative locations of the sites on a single tetrahedron to be, (in units of lattice constant a) $\mathbf{r}_0 = (1/8, 1/8, 1/8)$, $\mathbf{r}_1 = (1/8, -1/8, -1/8)$, $\mathbf{r}_2 = (-1/8, 1/8, -1/8)$ and $\mathbf{r}_3 = (-1/8, -1/8, 1/8)$. Symmetry considerations dictate that \mathbf{J}_{ij} and \mathbf{g}_i are completely described by four and two scalars respectively. \mathbf{J}_{ij} depends only on the sublattices that i, j belong to (similarly \mathbf{g}_i depends only on the sublattice of site i), and thus we use the notation in terms of $i, j = 0, 1, 2, 3$. Also, since $\mathbf{J}_{ij} = \mathbf{J}_{ji}^T$, only the $i < j$ matrices are written out. The \mathbf{J}_{ij} matrices are,

$$\mathbf{J}_{01} \equiv \begin{pmatrix} J_2 & J_4 & J_4 \\ -J_4 & J_1 & J_3 \\ -J_4 & J_3 & J_1 \end{pmatrix} \quad \mathbf{J}_{02} \equiv \begin{pmatrix} J_1 & -J_4 & J_3 \\ J_4 & J_2 & J_4 \\ J_3 & -J_4 & J_1 \end{pmatrix}$$

$$\mathbf{J}_{03} \equiv \begin{pmatrix} J_1 & J_3 & -J_4 \\ J_3 & J_1 & -J_4 \\ J_4 & J_4 & J_2 \end{pmatrix} \quad \mathbf{J}_{12} \equiv \begin{pmatrix} J_1 & -J_3 & J_4 \\ -J_3 & J_1 & -J_4 \\ -J_4 & J_4 & J_2 \end{pmatrix}$$

$$\mathbf{J}_{13} \equiv \begin{pmatrix} J_1 & J_4 & -J_3 \\ -J_4 & J_2 & J_4 \\ -J_3 & -J_4 & J_1 \end{pmatrix} \quad \mathbf{J}_{23} \equiv \begin{pmatrix} J_2 & -J_4 & J_4 \\ J_4 & J_1 & -J_3 \\ -J_4 & -J_3 & J_1 \end{pmatrix} \quad (\text{S2})$$

Defining $g_+ = \frac{1}{3}(2g_{xy} + g_z)$ and $g_- = \frac{1}{3}(g_{xy} - g_z)$, the \mathbf{g}_i matrices read as,

$$\mathbf{g}_0 \equiv \begin{pmatrix} g_+ & -g_- & -g_- \\ -g_- & g_+ & -g_- \\ -g_- & -g_- & g_+ \end{pmatrix} \quad \mathbf{g}_1 \equiv \begin{pmatrix} g_+ & g_- & g_- \\ g_- & g_+ & -g_- \\ g_- & -g_- & g_+ \end{pmatrix}$$

$$\mathbf{g}_2 \equiv \begin{pmatrix} g_+ & g_- & -g_- \\ g_- & g_+ & g_- \\ -g_- & g_- & g_+ \end{pmatrix} \quad \mathbf{g}_3 \equiv \begin{pmatrix} g_+ & -g_- & g_- \\ -g_- & g_+ & g_- \\ g_- & g_- & g_+ \end{pmatrix} \quad (\text{S3})$$

The interaction part when written in terms of spin directions along the local [111] axes (denoted by S), is,

$$H_{int} = \sum_{\langle i,j \rangle} (2 - \lambda) J_{zz} S_i^z S_j^z - \lambda J_{\pm} (S_i^+ S_j^- + S_i^- S_j^+) \\ + \lambda J_{\pm\pm} (\gamma_{ij} S_i^+ S_j^+ + \gamma_{ij}^* S_i^- S_j^-) \\ + \lambda J_{z,\pm} [S_i^z (S_j^+ \zeta_{ij} + S_j^- \zeta_{ij}^*) + i \leftrightarrow j] \quad (\text{S4})$$

where $J_{zz}, J_{\pm}, J_{\pm\pm}, J_{z,\pm}$ are couplings and the parameter λ has been introduced by us to tune from the classical ice manifold ($\lambda = 0$) to real material relevant parameters ($\lambda = 1$). ζ_{ij} and γ_{ij} are bond dependent phases,

$$\zeta \equiv \begin{pmatrix} 0 & -1 & e^{+i\pi/3} & e^{-i\pi/3} \\ -1 & 0 & e^{-i\pi/3} & e^{+i\pi/3} \\ e^{+i\pi/3} & e^{-i\pi/3} & 0 & -1 \\ e^{-i\pi/3} & e^{+i\pi/3} & -1 & 0 \end{pmatrix} \gamma = \zeta^* \quad (\text{S5})$$

The relation between J_1, J_2, J_3, J_4 and $J_{zz}, J_{\pm}, J_{\pm\pm}, J_{z,\pm}$ is,

$$J_{zz} = -\frac{1}{3}(+2J_1 - J_2 + 2J_3 + 4J_4) \\ J_{\pm} = +\frac{1}{6}(+2J_1 - J_2 - J_3 - 2J_4) \\ J_{\pm\pm} = +\frac{1}{6}(+J_1 + J_2 - 2J_3 + 2J_4) \\ J_{z\pm} = +\frac{1}{3\sqrt{2}}(+J_1 + J_2 + J_3 - J_4) \quad (\text{S6})$$

We provide a table of the parameters that were used for the calculations in both notations. For $\text{Yb}_2\text{Ti}_2\text{O}_7$ (YbTO), parameters from Ref. [3] and Ref. [24], and for $\text{Er}_2\text{Ti}_2\text{O}_7$ (ErTO), parameters from Ref. [27] were used. The parameters from one notation are directly converted to the other notation (without accounting for error bars) unless already provided in the reference.

II. DETAILS OF THE NUMERICAL CALCULATIONS

The 32 site cluster studied in the paper, has 2 cells in each direction of the FCC primitive lattice vectors. The view of this cluster along the global [111] direction, and the directions in which the periodic boundary conditions are applied have been shown in Fig. 1 of the main text. We have employed its translational symmetries with momentum directions labelled $\mathbf{k} = (k_1, k_2, k_3)$, the former two representing translations perpendicular to the global [111] direction and the latter along [111]. For the 32 site cluster each $k_i = 0$ or $k_i = \pi$ giving rise to a total of 8 momentum sectors. The Hilbert space in each momentum sector is approximately 536 million dimensional. In Fig. 3 and Fig. 5 of the main text, the lowest lying energies are mapped out in all 8 momentum sectors as a function of parameters in the Hamiltonian (field for Fig. 3 and λ for Fig. 5).

Parameter set	J_1 (meV)	J_2 (meV)	J_3 (meV)	J_4 (meV)	J_{zz} (meV)	J_{\pm} (meV)	$J_{z\pm}$ (meV)	$J_{\pm\pm}$ (meV)	g_{xy}	g_z
YbTO Ref. [3]	-0.09	-0.22	-0.29	+0.01	0.17	0.05	-0.14	0.05	4.32	1.8
YbTO Ref. [24]	-0.028	-0.326	-0.272	+0.049	0.026	0.074	-0.159	0.048	4.17	2.14
ErTO Ref. [27]	+0.115	-0.056	-0.099	-0.003	-0.025	0.065	-0.0088	0.042	5.97	2.45

Table I. Parameter sets used in the paper in two notations for YbTO and ErTO. The reported parameters from one notation are directly converted to the other notation (without accounting for error bars) unless already provided in the reference.

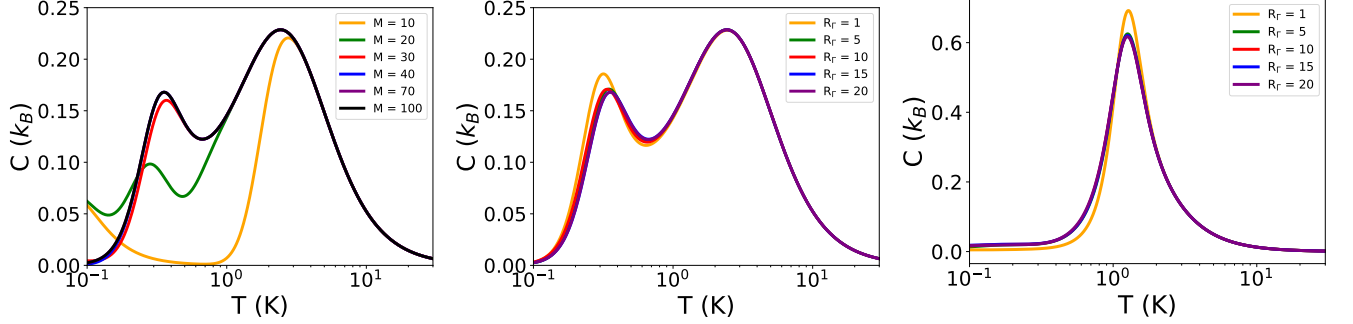


Figure S1. (Color online): Convergence of the heat capacity profiles (per mole of the magnetic ion) on the 32 site pyrochlore cluster as a function of temperature. The left panel shows results for YbTO for increasing M for fixed $R_\Gamma = 15$ ($R = 120$ total seeds). The center and right panels show results for increasing R_Γ (for fixed $M = 100$) for YbTO and ErTO respectively.

Calculations with each starting random vector took roughly 10 hours on 48 cores on the MARCC supercomputer for $M = 100$ Lanczos iterations. Larger number of iterations were needed ($M = 200 - 400$) for studying low energy spectra. Observables that commute with the Hamiltonian (such as the specific heat) are calculated using the formulae [23],

$$\langle A \rangle = \frac{1}{Z} \sum_{\Gamma} \frac{N_{\Gamma}}{R_{\Gamma}} \sum_{r=1}^{R_{\Gamma}} \sum_{j=1}^M \exp(-\beta E_{jr}) |\langle r | \psi_{jr} \rangle|^2 A_{jr} \quad (S7)$$

$$Z = \sum_{\Gamma} \frac{N_{\Gamma}}{R_{\Gamma}} \sum_{r=1}^{R_{\Gamma}} \sum_{j=1}^M \exp(-\beta E_{jr}) |\langle r | \psi_{jr} \rangle|^2 \quad (S8)$$

where β is the inverse temperature, Γ is a symmetry (sector) index, N_{Γ} is the (sector) Hilbert space size, $|r\rangle$ is a random vector (in the given sector) used to start the Lanczos iteration, R_{Γ} is the number of such starting vectors, ψ_{jr} is the j^{th} eigenvector obtained after M iterations (with $|r\rangle$ as the start vector), E_{jr} is the corresponding Ritz eigenenergy and $A_{jr} = \langle \psi_{jr} | A | r \rangle / \langle \psi_{jr} | r \rangle$

In the main text, we also mentioned that the finite temperature Lanczos method (FTLM) works well because only a small number of Krylov space vectors (M) and starting vectors (R_{Γ} in every symmetry sector) are needed to obtain accurate results. (Note that since there are 8 symmetry sectors, $R = 8R_{\Gamma}$). To validate this claim we show the convergence properties by varying M and fixed R_{Γ} , and varying R_{Γ} at fixed M in Fig. S1.

For example, Fig. S1 shows our results for YbTO when we fix $R_{\Gamma} = 15$ and vary M . As expected, the high temperature features converged the fastest with increasing M , for example, the entire Schottky anomaly centered at 2.4 K converges by $M = 20$. By $M = 50$ other lower temperature features have

also converged, this is verified by going all the way to $M = 100$.

In the central panel, we fix $M = 100$ and vary R_{Γ} . It is remarkable that a single random vector per sector $R_{\Gamma} = 1$ is sufficient for reasonably representing the Schottky anomaly. However, to obtain other features quantitatively, one needs $R_{\Gamma} \geq 5$ to converge features on the log scale shown. Finer features associated with the "peak" at $T \approx 0.34$ K show small variations (0.02 K) between $R_{\Gamma} = 5$ to $R_{\Gamma} = 15$ but converge by $R_{\Gamma} = 20$. The right panel of the figure shows analogous results for ErTO.

III. COMPARISON OF MAGNETIZATION PROFILES

In the main text, we showed representative magnetization (M) profiles as a function of temperature (T) as part of Fig. 4. Here we clarify that quantum effects are crucial for explaining the trends seen in recent experiments in a [111] magnetic field [16].

Fig. S2 shows our results for two field strengths (h). At low temperatures, M vs T is relatively flat, a feature captured quantum mechanically but not classically. Moreover, at $h = 0.055$ T the classical kink in the magnetization is at much higher temperature, consistent with a larger T_c seen classically. In addition, classically, the change in M with T is more rapid in the paramagnetic regime in comparison to experiments.

In contrast, the quantum calculations largely agree with experiments and correct both these discrepancies. The mild disagreements with experiments are attributed to a combination of finite size effects, inaccurate parameters and presence of

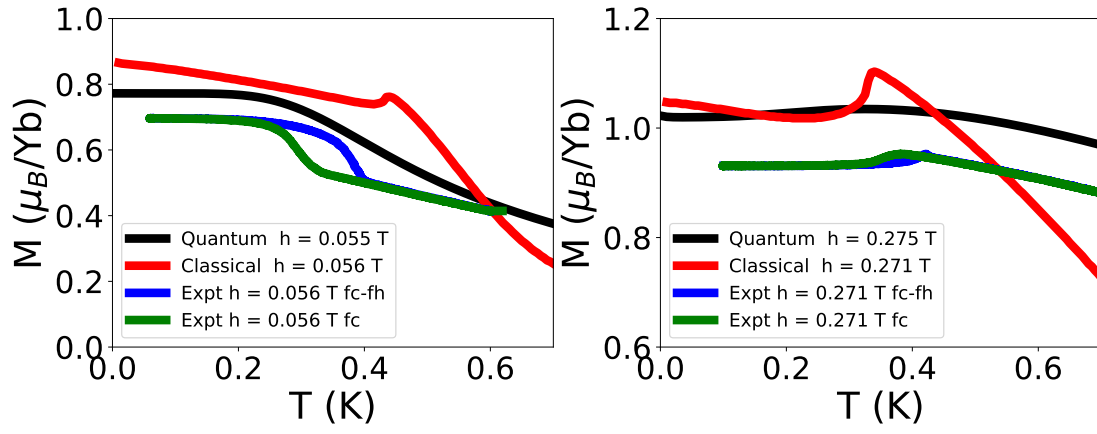


Figure S2. (Color online): Quantum and classical magnetization (M), measured along the same direction as the applied [111] magnetic field (h) versus temperature (T). Comparisons are made to two experimental profiles (with similar field values), left for $h = 0.055$ T and right for $h = 0.275$ T. fc and fh refer to field cooled and field heated measurements respectively.

magnetic domains in real systems.